IEEE Access
Multidisciplinary | Rapid Review | Open Access Journal

Received March 29, 2020, accepted April 9, 2020, date of publication April 15, 2020, date of current version April 30, 2020.

Digital Object Identifier 10.1109/ACCESS.2020.2988072

Co-Located Self-Neutralized Handset Antenna Pairs With Complementary Radiation Patterns for 5G MIMO Applications

CHONG-ZHI HAN[1,2], LI XIAO[3], ZHE CHEN[1,2], (Member, IEEE), AND TAO YUAN[1,2], (Member, IEEE)

[1]ATR National Key Laboratory of Defense Technology, College of Information Engineering, Shenzhen University, Shenzhen 518060, China
[2]Guangdong Provincial Mobile Terminal Microwave and Millimeter-Wave Antenna Engineering Research Center, College of Electronics and Information Engineering, Shenzhen University, Shenzhen 518060, China
[3]Shenzhen Academy of Information and Communications Technology, Shenzhen 518026, China

Corresponding author: Li Xiao (xiaoli@caict.ac.cn)

This work was supported by the Shenzhen Basic Research Projects under Grant JCYJ20170413151115990 and Grant JCYJ20180305124721920.

ABSTRACT In this paper, 4 × 4 / 8 × 8 / 10 × 10 multiple input multiple output (MIMO) antenna systems composed of co-located self-neutralized antenna pairs are proposed to operate at 4.8-5.0 GHz (part of N77 band) for the fifth-generation (5G) communication applications. The proposed antenna pairs consist of a loop antenna and a monopole antenna, co-locating together with a compact size of 6.7 × 15.5 × 3.08 mm^3. Meanwhile, the co-located design can miniaturize 50% of the antenna size, which is quite significant for practical mobile applications with limited space environment. In addition, the adoption of the self-neutralization technique between the co-located loop antenna and the monopole antenna contributes to a satisfactory isolation with better than 25 / 20 / 16.5 dB for the 4 × 4 / 8 × 8 / 10 × 10 MIMO systems respectively. Analysis of the isolation improvement is also discussed in this study. Moreover, the antenna pairs are able to generate complementary radiation patterns, enabling the envelope correlation coefficients (ECC) between the antennas to be less than 0.1. Also, efficiencies of the MIMO antenna system achieve up to 60% as there is no external decoupling structure deteriorating the radiation performance of the proposed antenna pairs. Finally, a 4 × 4 MIMO antenna system prototype is fabricated and measured to verify its prospect for 5G MIMO applications.

INDEX TERMS Complementary radiation pattern, fifth-generation (5G), MIMO antenna, mobile antenna, self-neutralization.

NOMENCLATURES AND ABBREVIATIONS

5G:	fifth-generation;
MIMO:	multiple input multiple output;
ECC:	envelope correlation coefficients;
DCS:	digital cellular system;
UMTS:	universal mobile telecommunications system
WLANs:	wireless local area networks;
DGS:	defect ground structure;
LTE:	long term evolution;
N77 band:	3.3-4.2 GHz;
N79 band:	4.4-5.0 GHz;

The associate editor coordinating the review of this manuscript and approving it for publication was Walid Al-Hussaibi.

I. INTRODUCTION

With the increasing demand on higher channel capacities and data rate in the mobile communication, the 5G MIMO research has been attracted much more attention among these days. Potential Sub-6 GHz frequency bands such as 3.3-3.6 GHz and 4.8-5.0 GHz have been assigned for 5G mobile communication in several countries such as China, which is believed that the infrastructures operating in this bands will be deployed soon. Hence, many handset MIMO antenna designs for 5G Sub-6 GHz have been reported recently [1]–[9]. Among these designs, the isolations and ECCs between adjacent antenna elements are the key considerations, especially when the designs are implemented within a limited region in the mobile phones. Generally, it is

contradictory to achieve high isolation among MIMO antenna elements and miniaturize the size of handsets. In addition, the radiation pattern of each elements in the MIMO system would affect the ECC significantly. Overall, the abovementioned problems increase the antenna design challenge in mobile terminals particularly when the available space is limited.

To enhance the isolation, several techniques have been demonstrated in literatures. Neutralization line was firstly proposed for isolation enhancement in DCS1800 and UMTS bands [10]. Subsequently, the method was applied to MIMO antenna system to achieve 9-dB isolation improvement between two WLANs antennas 7-mm away from each other [11]. Nevertheless, the approach is lack of intuitionistic design procedure, and particularly, the neutralization line is typically suitable for narrow band decoupling and would also incur mismatch problem simultaneously. DGS [12] and resonator-based approach (decoupling element) [13], [14] can also mitigate the coupling between closely arranged antenna elements. The multi-mode decoupling technique with tunable characteristic for mobile terminals is also achieved by introducing different decoupling elements in [14], which is of great significance for the mobile multiband antennas. However, the DGS and the resonator-based methods would decrease the total efficiency of the designed antennas, degrading their potential applications in mobile terminals. Introducing a decoupling network in handset is another way to achieve mobile terminal antenna decoupling [15], [16]. Nevertheless, the design complexity of the network increases significantly once more antenna elements have to be decoupled, and the layout also becomes intricate within a limited area in mobile terminals.

In another respect, antenna performance with handhold effect determines whether the antenna is suitable for applying in industrial mobile terminals, as the handhold effect is directly relevant to the practical user experience. Antennas proposed in [4]–[6], [14] and [9], [17]–[21] have proved that the antenna performance definitely decreases with users' handholding. Particularly, the efficiency of the antenna near the user's hands would drop from 30% to 20% in [14], and the antenna efficiency mentioned in [17] decreased to 30% at LTE high bands. Normally, the strategy to decrease the handhold performance drop is to avoid directly touch between radiation elements and the users' hands. From this aspect, co-located antenna pairs could shrink the total size of the MIMO antenna system, which would introduce more freedom to arrange the radiation elements. And the smaller overall size may avoid the directly interference with human body. However, the co-located antenna pair may suffer severe coupling effects, considering the limited space between different antenna elements. Hence, new technique should be proposed to enhance the isolation between the co-located antenna pairs. Recently, several works propose compactly arranged MIMO antennas/antenna pairs to miniaturize the overall sizes of the MIMO antenna system [22]–[27]. Among these designs, [22]–[25] achieve bandwidth of 3.4-3.6 GHz to cover part of N77 band with 12.7-20 dB isolation performance. Also, wider bandwidth can be obtain in [26], [27] at the expense of relatively lower isolation (10.5-12 dB) performance. In these works, Orthogonal-mode and common/differential-mode are adopted to achieve decoupling/self-decoupling effect. However, the isolation in these literatures are hard to exceed 20 dB. Hence, the 20-dB isolation among antennas seems to be a bottleneck for 5G terminal MIMO antenna systems.

In this paper, a novel co-located self-neutralized antenna pair (one loop antenna and one monopole antenna) with complementary radiation patterns covering part of N79 band for 5G MIMO applications is proposed to achieve desirable MIMO performance. The contributions of the paper can be summarized into three aspects. Firstly, the co-located design can miniaturize 50% of the antenna size, achieving spatial reuse. Although the spatial reuse is achieved in [22]–[24], [26], [27], the proposed co-located antenna pair is superior to these designs in terms of port distance. Our design shrined the distance to merely 3.2 mm. Secondly, the isolations among the 4×4 MIMO antenna system composed of two identical antenna pairs are better than 25 dB (superior to other published works) without any external decoupling/resonator element, since the self-neutralization mechanism is proposed in the paper. Moreover, the method to optimize the isolation between the co-located antenna pair is also discussed to further verify the "self-neutralization" technique in the paper, which is also distinguished from that in [22]–[27]. Thirdly, both of the loop antenna and the monopole antenna can obtain complementary radiation patterns because of the orthogonal current distribution along the radiating elements, which is of great significance for the MIMO antenna system. For further performance verification, the proposed antenna pairs are adopted to realize 4×4 / 8×8 / 10×10 MIMO systems within a limited area of 76×150 mm^2. Finally, small ground clearance is needed in this work, enabling the antenna pairs more suitable in practical handset environment.

This paper is organized as follows: In section II, the "self-neutralization mechanism" is addressed to interpret the operating mechanism of the co-located self-neutralized antenna pair. Also, the structure optimization is discussed in this section. In section III, the arrangements of the antenna pair are studied by simulation to verify the MIMO performance of the proposed co-located antenna pair as well as the "self-neutralization mechanism". And the antenna performance in practical application environments is also discussed. In section IV, a 4 MIMO antenna system is fabricated and measured. Finally, Section V draws a conclusion.

II. ANTENNA DESIGN FOR 4 × 4 MIMO SYSTEM

A. GEOMETRY OF THE PROPOSED ANTENNA PAIRS AND MIMO SYSTEM

It is interesting to note that the design idea of the co-located antenna comes from an artistic statue as shown in Fig. 1(a), which consists of a circular loop and an L-shaped rod. As an

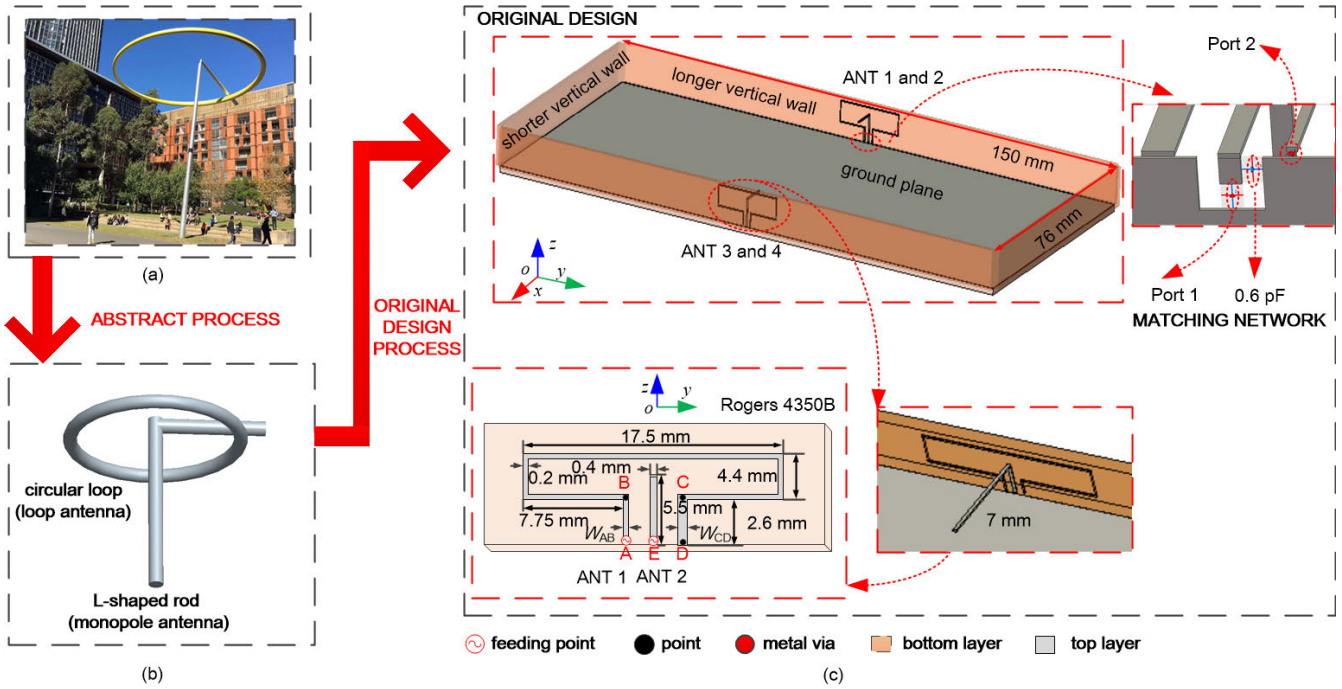

FIGURE 1. (a) An artistic statue located in Central Park Sydney (photo courtesy of Dr. Wei Lin from UTS); (b) The abstract process of the artistic statue; (c) Configuration of the original antenna pair and the corresponding 4 × 4 MIMO handset antenna system.

abstraction, the circular loop refers to the loop antenna and the L-shaped rod indicates the monopole antenna in our design, which is shown in Fig. 1(b). When the loop antenna works at one-wavelength mode, the coupling between the loop antenna and the monopole antenna can reach a self-neutralization status. Then, the original co-located antenna pair, as well as the corresponding 4×4 MIMO antenna system are illustrated in Fig. 1(c). For the original design, a monopole antenna and a loop antenna are purposely designed to be co-located to realize antenna miniaturization without occupying any extra region. The antenna is mainly configured in *xoy* and *yoz*-planes, and no additional ground clearance in *xoy*-plane is necessary. For the 4×4 MIMO antenna system, the original antenna pairs are symmetrically placed along the two longer walls of a 76×150 mm^2 ground plane, the size of which is typically used in practical mobile terminal. The ground plane and other four vertical walls representing the handset frame are all printed on a 1.52 mm thick Rogers 4350B substrate with relative permittivity 3.48 and loss tangent 0.0037. The antenna pairs along the two longer walls are named ANTs 1, 2, 3 and 4 respectively (ANTs 1and 3 are loop antennas; ANTs 2 and 4 are monopole antennas).

Take ANT 1 and ANT 2 of the original design to better illustrate the structure of the proposed antenna pairs, where the ANT 1 is fed at point A, and point D is the shorting point. ANT 1 can be considered as a transformed inverted-U-shaped loop antenna with a height of 7 mm. ANT 2 is an L-shaped monopole antenna placed at the center of the ANT 1. The vertical strip of ANT 2 is 5.5 mm along the *z*-axis and the horizontal part has a length of 7 mm which is perpendicular to the loop antenna. To achieve a 4×4 MIMO antenna system, only 2 antenna pairs are needed along vertical walls, which are particularly arranged at the center of the two longer walls of the handset frame in this design, leaving enough space for allocating LTE and millimeter wave antennas (if necessary in future) in practical applications. According to a typical handset model, the size of the ground plane is set to 76×150 mm^2 in this work. Full-wave electromagnetic analysis is performed by using the commercial software CST Microwave Studio to analyze the antenna structure, results of which will be discussed in the following subsections.

B. SELF-NEUTRALIZATION MECHANISM

Fig. 2 presents the vector surface current distributions of the antenna pair at the resonant frequency. Fig. 2(a) shows the circumstance that the ANT 1 (loop antenna) is excited from the point A while the ANT 2 (monopole antenna) is terminated with a 50 Ω load at point E. The vector surface current distributions along the ANT 1 are similar to a cosine curve, which can be considered as "active current" generated from the point A, while the current along the ANT 2 is coupled from the ANT 1, which in turn can be deemed as "passive current" (coupling current). Note that the "active current" refers to current excited directly by the feeding source; the "passive current" can be regarded as current caused by coupling effect. The active current along the ANT 1 makes it resonate at a one-wavelength mode, which can be observed from Fig. 2(a). Another working state of the proposed antenna pair is under the circumstance that the ANT 2 is excited at point the E while the ANT 1 is terminated with a 50 Ω load at

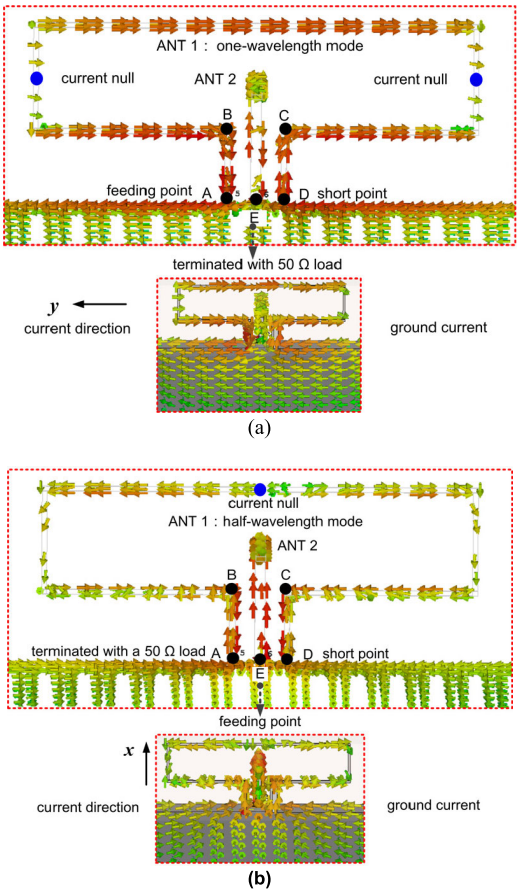

FIGURE 2. **Vector surface current distributions of the co-located antenna pairs at 4.9 GHz. (a) Loop antenna under excitation; (b) Monopole antenna under excitation.**

the point A, as shown in Fig. 2(b). For this case, the current along the ANT 2 transforms to ''active current'' excited at the point E and that along the ANT 1 is ''passive current'' coupled from the ANT 2. In this circumstance, the ANT 1 works as half-wavelength mode.

One can observe from Fig. 2(a) that the ANT 1 works as one-wavelength mode and the coupling (''passive'') current along the ANT 2 is relatively weak. This phenomenon can be explained in three aspects. Firstly, the active one-wavelength mode of the ANT 1 (loop antenna) generates lower resonant frequency compared with the half-wavelength mode which is excited by the coupling effect from the ANT 2 (monopole antenna). Namely, the active and passive current distribution along the ANT 1 act as different modes. Hence, the coupling current from the ANT 2 would not deteriorate the performance of the ANT 1 effectively, which means better isolation can be obtained by the proposed antenna pair. The second aspect which leads to better isolation between the ANT 1 and the ANT 2 can be demonstrated by the ground current distribution shown in Fig. 2. The ground current is along *y*-axis direction when the ANT 1 is excited, as shown in Fig. 2(a); while that is along *x*-axis direction under the circumstance that the ANT 2 is fed as plotted in Fig. 2(b). Hence, the orthogonal ground current distribution can be obtained, resulting in a weak ground coupling of the proposed antenna pair. Thirdly, the currents along strip-A-B and strip-C-D obtain anti-phase on the condition that the loop antenna works at one-wavelength mode. Hence, the coupling from the ANT 1 to the ANT 2 can be neutralized. The phenomenon can further enhance the isolation between the antenna elements within the same antenna pair, which is named as ''self-neutralization'' in the paper.

To further elaborate the working mechanism of the self-neutralization technique utilized in this work, a simplified model of the original antenna pair is depicted in Fig. 3. Note that the two-port network consisting of ANTs 1 and 2 is reciprocal (the medium between the ANTs 1 and 2 is linear, passive, and isotropic), i.e., $S_{12} = S_{21}$. And the figure describes the circumstance that the ANT 1 (loop antenna) is excited while the ANT 2 (monopole antenna) is terminated with 50 Ω load at point E. When the ANT 1 is excited from the point A, the current goes along the loop strip to the shorting point D which is connected to the ground plane. The vector surface current distribution along the ANT 1 is marked by red arrows with two current null points located at the center of the vertical parts of the loop strip. The current along the path-A-B is denoted as $\vec{I}_{AB}$ and that of the path-C-D is $\vec{I}_{CD}$. The coupling current caused by $\vec{I}_{AB}$ and $\vec{I}_{CD}$ are $\vec{I}_{\mathrm{AB}}{}'$ ($\vec{I}_{\mathrm{AB}}{}' = k_1 \times \vec{I}_{\mathrm{AB}}$) and $\vec{I}'_{\mathrm{CD}}$ ($\vec{I}_{\mathrm{CD}}{}' = k_2 \times \vec{I}_{\mathrm{CD}}$) respectively. As ANT 2 is terminated with 50 Ω, the current ($\vec{I}_{21}$) along the ANT 2 is just the coupling current from ANT 1, i.e., $\vec{I}_{21} = \vec{I}_{\mathrm{AB}}{}' + \vec{I}_{\mathrm{CD}}{}' = k_1 \times \vec{I}_{\mathrm{AB}} + k_2 \times \vec{I}_{\mathrm{CD}}$. Hence, due to the opposite phase between $\vec{I}_{AB}$ and $\vec{I}_{CD}$, $\vec{I}_{21}$ becomes extremely weak, which means good isolation performance can be obtained by the proposed antenna pair. It should be emphasized that the proposed self-neutralization method does not require extra structure to reduce the coupling effect between the antennas. On the contrary, the coupling currents between the antenna elements of one antenna pair are properly arranged to neutralize with each other. Moreover, the antenna pairs occupy nearly the same region as a single loop antenna in *yoz*-plane. Hence, the proposed co-located

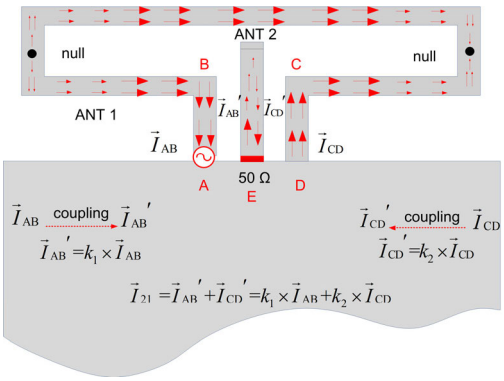

FIGURE 3. **Simplified model of self-neutralization for the proposed antenna pairs (the loop antenna is excited while the monopole antenna is terminated with 50 Ω load).**

antenna pair and the decoupling technique is very suitable for compactly arranged handset MIMO antennas. Note that the proposed "self-neutralization" can only be achieve under two conditions: ① the proposed loop antenna should work as one-wavelength mode; ② the proposed monopole antenna should be arranged between the feeding strip and ground strip of the loop antenna approximately to achieve "self-neutralization".

C. ISOLATION OPTIMIZATION

The self-neutralization characteristic of this design provides a decent isolation. To further enhance the isolation, we could balance the current amplitudes along path A-B and patch C-D by tuning the width of the loop antenna. When W_{AB} remain unchanged, the current amplitude variation along path C-D with different W_{CD} and the corresponding isolation are shown in Fig. 4 and Fig. 5, respectively. In the simulation, current with a normalization amplitude 1 is excited at the point A using the commercial simulation software CST Microwave Studio. And the current at the point D varying against frequency can also be observed in Fig. 4.

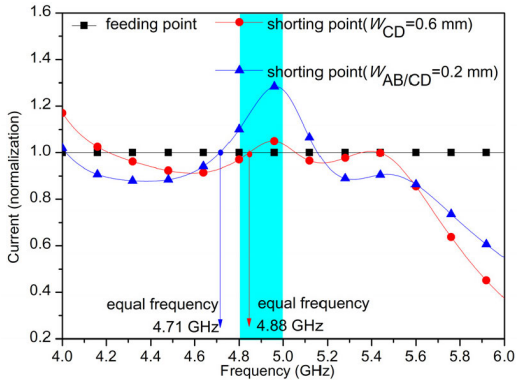

FIGURE 4. The simulated current amplitude versus frequency with different values of W_{CD}. (The value of W_{AB} is fixed at 0.2 mm when varying the value of W_{CD}).

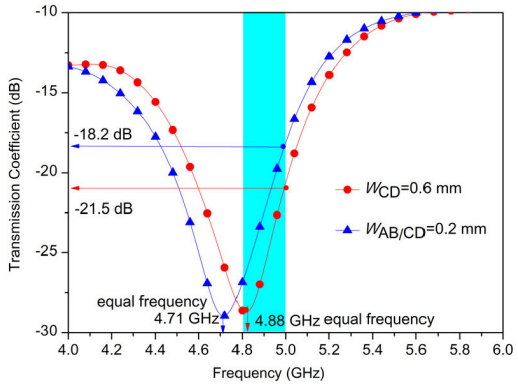

FIGURE 5. The simulated transmission coefficient of ANT 1 and ANT 2 with different values of W_{CD}. (The value of W_{AB} is fixed at 0.2 mm when varying the value of W_{CD}).

The isolation optimization can be detailed in following steps. Originally, the loop antenna is designed with symmetrical structure ($W_{AB} = W_{CD} = 0.2$ mm) and its corresponding numerical results are depicted by black and blue lines in Fig. 4. As can be seen that the current amplitudes become equivalent at the frequency of 4.71 GHz (hereinafter called "equal frequency" for convenience). Therefore, the simulated S_{12} gets its minimal value at nearly the same frequency, as shown in Fig. 5, which well agrees with the working mechanism of the self-neutralization technique as elaborated in the last subsection. In this circumstance, the frequency of the minimal S_{21} is not covered by the desired band of 4.8-5.0 GHz (light blue area in Figs. 4 and 5), while the inband isolation is only above 18.2 dB. Then, to enhance the isolation performance at 4.8-5.0 GHz, the equal frequency should be optimized into the desired band. Analysis shows that different widths of strip-C-D lead to different impedance response, which would vary the value of I_{CD} shown in Fig. 3. Hence, currents of both the points A and D with different W_{CD} are also studied and illustrated in Fig. 4. Current at the point D (shorting point) gets weaker in the desired band with $W_{CD} = 0.6$ mm compared with that of $W_{CD} = 0.2$ mm, and the equal frequency shifts into the desired band accordingly. At last, the corresponding simulated S_{21} has been depicted in Fig. 5. Better isolation from 18.2 dB to 21.5dB can be obtained with W_{CD} shifting from 0.2 mm to 0.6 mm. As a result, it is shown that the isolation between the ANT 1 and the ANT 2 can be optimized by adjusting the width of strip-C-D.

D. STRUCTURE OPTIMIZATION AND SIMULATED PERFORMANCE

For the original antenna pair and corresponding 4 × 4 MIMO antennas system, full-wave electromagnetic analysis is performed by using the commercial software CST Microwave Studio. For better input impedance matching, the ANTs 2 and 4 require a 0.8 pF capacitor in parallel to optimize the reflection coefficient. Additionally, the −10 dB reflection coefficient bandwidth of ANTs 1, 2, 3 and 4 are wide enough to cover the bandwidth of 4.8-5.0 GHz as shown in Fig. 6.

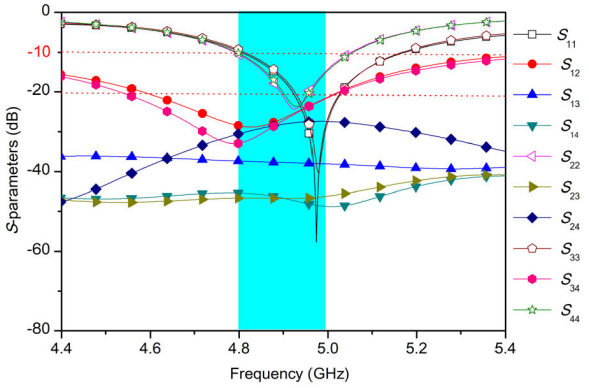

FIGURE 6. Simulated *S*-parameters of the original design.

In the case of the original design and the 4 × 4 MIMO antennas system as illustrated in Fig. 1, isolation between the two antennas of one antenna pair (e.g., ANT 1 and ANT 2) is the key factor which may cause deterioration on the whole

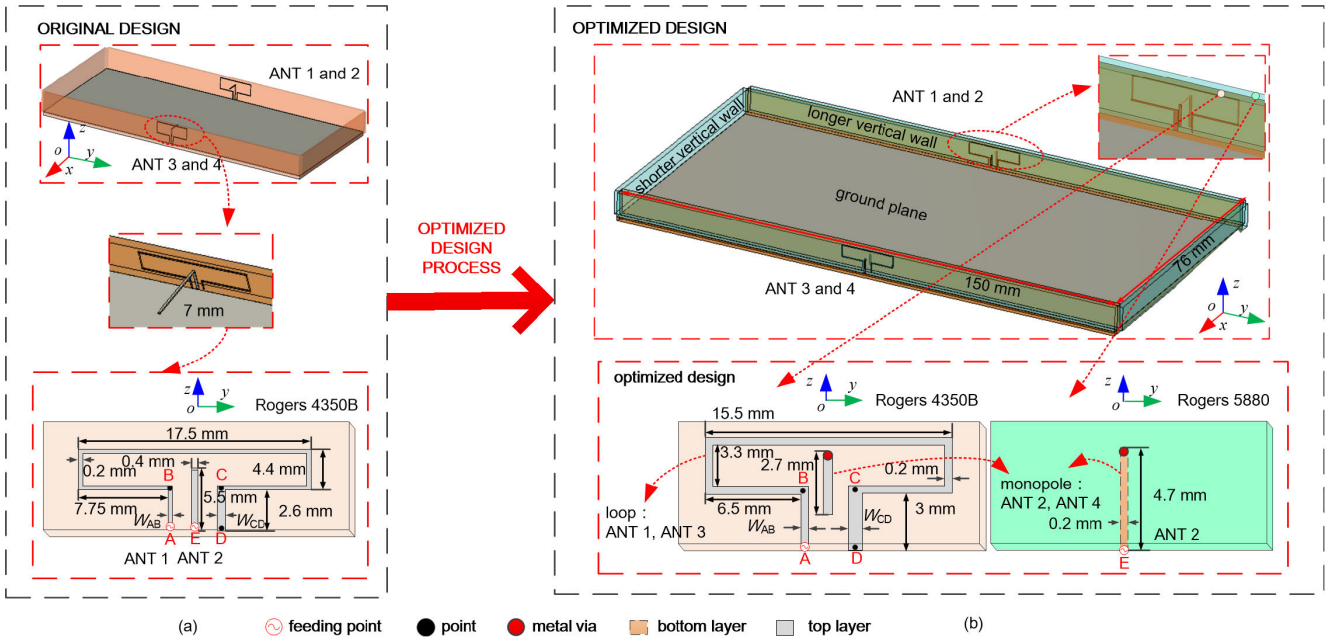

FIGURE 7. (a) Configuration of the original antenna pair and the corresponding 4 × 4 MIMO handset antenna system; (b) Configuration of the optimized antenna pair and the corresponding 4 × 4 MIMO handset antenna system.

MIMO antenna system. Hence, ANTs 1, 2, 3 and 4 are studied to evaluate the MIMO system performance via simulation. S_{12} and S_{34} stand for the isolation level of the two antenna pairs. S_{12} and $S_{34} < -21.5$dB within the band of 4.8-5.0 GHz can be obtained with a co-located design, which provides more design freedom for the terminal MIMO antenna system. Additionally, isolations between different antenna pairs can be observed from curves of S_{13}, S_{24}, S_{23}, and S_{14}, respectively. Clearly, the isolation between ANTs 1 and 3 (two loop antennas, $S_{13} < -35$ dB) are higher than that between ANTs 2 and 4 (two monopole antennas, $S_{24} < -25$ dB). This is because that ANTs 1 and 3 mainly work as balance mode (one-wavelength mode), while ANTs 2 and 4 (monopole antennas) operate as unbalance mode (quarter-wavelength mode) [28]. The ground current distribution of the balance mode is less than that of the unbalance mode. As a result, the coupling caused by the ground current leads to the different isolation. Similarly, isolations between ANT 1/3 and ANT 4/2 in different antenna pairs (S_{14}, $S_{32} < -45$ dB) are better than that of ANTs 2 and 4 ($S_{24} < -25$ dB) within the desired band.

Throwing an insight into the original design, two aspects should be optimized to improve its performance for the 5G mobile terminal applications. Firstly, the isolation among the 4×4 MIMO antennas system which is composed of the original design can be enhanced while considering that all other isolations (S_{13}, S_{14}, S_{23}, and S_{24}) are better than 25 dB except S_{12}. Hence, it is expected that the isolation (S_{12}) between the ANTs 1 and 2 (the loop antenna and the monopole antenna in one antenna pair) could be enhanced to the same level of that (S_{24}) between the ANTs 2 and 4 (two monopole antennas), which is 25 dB around. Another shortcoming of the original design is that the ANTs 2 and 4 have a 7 mm-strip along the x-axis, which may restrict the applications of the antenna pairs as the space available for antenna design is limited inside mobile terminals. To solve these problem, structure optimization is carried out to achieve antenna miniaturization and isolation enhancement simultaneously. The optimized design of the antenna pair is illustrated in Fig. 7(b), the structure of which consists of two printed circuit board (PCB) layers. The green one is a 1.57 mm thick Rogers 5880 substrate with relative permittivity 2.2, and the orange one is 1.52 mm thick Rogers 4350B with relative permittivity 3.48. The ANT 2/4 (monopole antenna) is etched on different PCB layers and a metal via with radius of 0.1 mm is utilized to act as the strip along the x-axis. Other parameters of the optimized design are also shrunk accordingly. Also, the enlarged feeding network view of the optimized antenna pair is illustrated in Fig. 8. Note that the ground plane is etched with copper at both the top and the bottom layers of the Rogers 4350B substrate, and the feeding network is arranged at the bottom layer. Metal via is used and clarified by yellow and red color. The metal via in yellow listed in Fig. 8 is utilized to connect two copper layers of the ground plane, enabling the proposed structure coincidence well with the realistic circumstance in practical handsets. To ensure the electric connection between the top and the bottom copper layers, the distance between the yellow via is set as 1 mm. Also, the metal via in red is used to act as parts of the antennas, making the antenna be seemed as the monopole antenna and the loop antenna. Moreover, a 1.5 nH inductor and a 1 pF capacitor are introduced to optimize the S-parameters of the

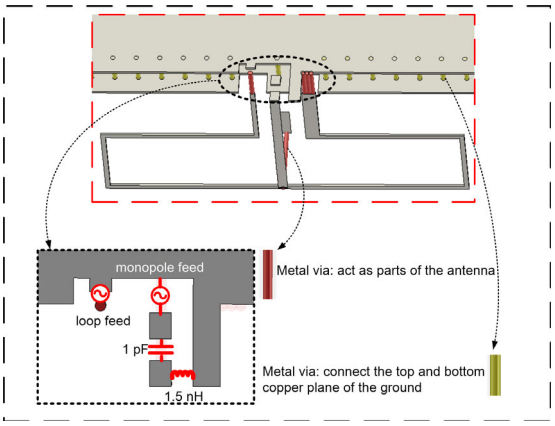

FIGURE 8. Enlarged feeding network view of the optimized antenna pairs.

monopole antenna. Also, the pads are utilized to introduce the above-mentioned 1.5 nH inductor and 1 pF capacitor onto the feeding network.

The optimized antenna pairs are analyzed in CST with results of S-parameters shown in Fig. 9. It can be seen that the isolation between the ANTs 1 and 2 are better than 25 dB and the S_{21} is nearly the same level as the S_{24}.

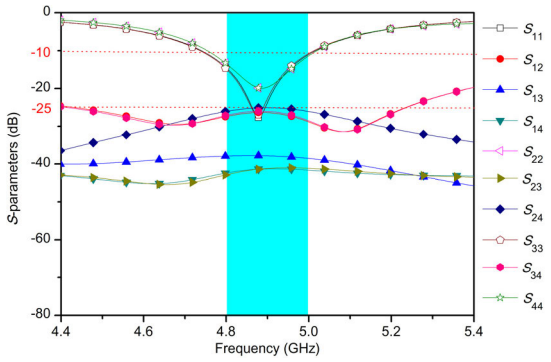

FIGURE 9. Simulated S-parameters of the optimized design.

Better isolation between the antenna pairs can ensure less interference coupled into the feeding points, reducing undesired resonance on the PCB. Moreover, for a co-located antenna pair, poor radiation isolation may cause a high risk to degrade its ECC performance as the two antennas radiate energy at precisely the same position. Typically, the ECC is calculated based on the equations (1) and (2), as shown at the bottom of this page, where $P_\theta(\Omega)$ and $P_\varphi(\Omega)$ denote the θ and φ polarization components of the incident field respectively, and χ presents the cross-polarization discrimination between

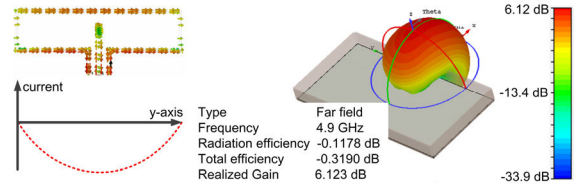

(a) Simulated radiation pattern of ANT 1 (loop antenna) at 4.9 GHz.

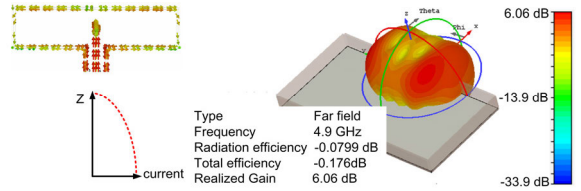

(b) Simulated radiation pattern of ANT 2 (monopole antenna) 4.9 GHz.

FIGURE 10. Radiation patterns of the optimized antenna pairs.

the two polarizations. According to (1) and (2), the ECC describes the radiation pattern envelope correlation between any two antennas. Hence, as the two antennas of the antenna pair proposed in this work can be considered as orthogonally co-locating with each other, their complementary radiation patterns are possible to generate lower ECC. To evaluate the ECC performance of the proposed optimized antenna pairs and 4 × 4 MIMO antenna system, the radiation patterns of ANT 1 (loop antenna) and ANT 2 (monopole antenna) in one antenna pair are demonstrated in Fig. 10. Owing to approximately orthogonal current distributions along the ANT 1 and ANT 2 (the ANT 1 has relative larger current amplitude along y-axis and that of ANT 2 is along x-axis), the approximately complementary radiation patterns are obtained. The simplified equivalent current distributions are also shown in Fig. 10, from which it can be seen that dense current exists along the y-axis and the z-axis for ANT 1 and ANT 2 respectively. Current source along the y-axis (ANT 1) produces omnidirectional far-field radiation patterns in the yoz-plane, and the far-field pattern of the ANT 2 is more likely omnidirectional in the xoy-plane with the current source shifting to z-axis. From the above analysis, the orthogonal radiation arms of both the ANT 1 and ANT 2 generate the complementary radiation patterns, helping the proposed antenna pairs achieve better MIMO performance. Furthermore, ECC values of the two different antennas are evaluated by simulation and shown in Fig. 11. Two ways to calculate the ECC values are utilized for comparison: one is the calculation based on far-field radiation data, and the other is to calculate the ECC values

$$\rho_{i,j} = \frac{\int (\frac{\chi}{1+\chi} E_{\theta,i}(\Omega) E^*_{\theta,j}(\Omega) P_\theta(\Omega) + \frac{1}{1+\chi} E_{\varphi,i}(\Omega) E^*_{\varphi,j}(\Omega) P_\varphi(\Omega)) d\Omega}{\sqrt{G_{e,i}} \sqrt{G_{e,j}}} \tag{1}$$

$$G_e = \int (\frac{\chi}{1+\chi} G_\theta(\Omega) P_\theta(\Omega) + \frac{1}{1+\chi} G_\varphi(\Omega) P_\varphi(\Omega)) d\Omega \tag{2}$$

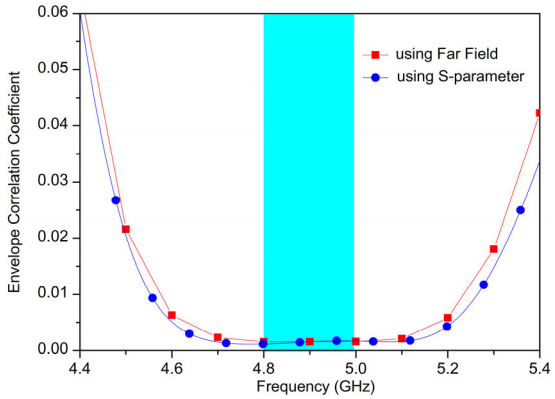

FIGURE 11. Simulated ECC of the proposed antenna pairs.

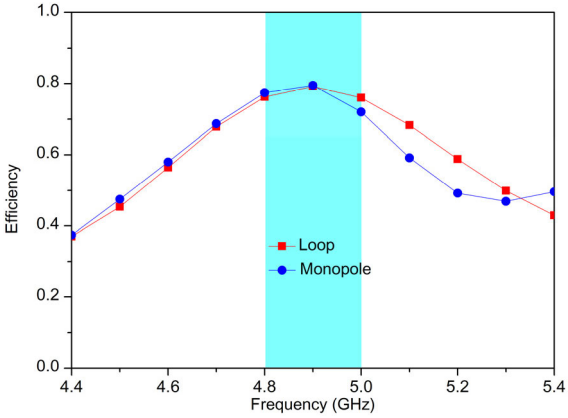

FIGURE 12. Simulated efficiencies of the proposed antenna pairs.

approximately using S-parameter. The ECC calculation from S-parameters follows the equation shown in (3). Both of the two calculated curves are plotted in Fig. 11, where the two curves coincide well with each other and the ECC lower than 0.01 inside the desired band can be observed.

$$\rho_{1,2} = \left| \frac{\left|S_{11}^* S_{12} + S_{21}^* S_{22}\right|}{\left[\left(1 - \left(|S_{11}|^2 + |S_{21}|^2\right)\right)\left(1 - \left(|S_{22}|^2 + |S_{12}|^2\right)\right)\right]^{0.5}} \right| \tag{3}$$

The efficiencies of the proposed antenna pairs are also studied with results shown in Fig. 12. Both of the ANT 1 and the ANT 2 obtain efficiencies up to 80%. Note that due to the symmetric arrangement of the antenna pairs, only one antenna pair is studied here to demonstrate the ECC and efficiency performance of the 4 × 4 MIMO antenna system.

E. USER HANDS EFFECT ON THE PROPOSED MIMO ANTENNA SYSTEM

It is known that user hands effect on handset antennas is a critical criterion to evaluate the antenna performance in practical environment. The performance of both single-handhold and double-handhold scenarios of the proposed 4 × 4 MIMO antenna system are studied in this subsection. Fig. 13 illustrates the modes of the proposed structure with user's hands holding. The radiation patterns of the two antenna pairs are also shown with realized gain. One can observe that radiation pattern distortion happens under the effect of user's hands for the ANTs 2 and 4 (monopole antennas). Also, the total efficiencies of the ANTs 2 and 4 are decreased by the handholding effect. The phenomenon can be traced to the unbalance mode of the monopole antennas. Whereas, the radiation performance of the ANTs 1 and 3 (loop antennas) are not affected severely due to their balance mode because only the ground plane is touched by the palm of the user's hands. The S-parameters of the single-handhold and double-handhold models are depicted in Figs. 14 and 15. A relatively distinct frequency shift of the ANTs 2 and 4 is observed in Figs. 14 and 15, which is mainly due to the user's hands effect. However, the −6 dB bandwidth of both the ANTs 1 and 2 (loop antennas) and ANTs 2 and 4 (monopole antennas) can still fulfill the operating band of 4.8-5.0 GHz with high isolation better than 23 dB.

The efficiencies and the ECCs are shown in Figs. 16 and 17 for the proposed 4 × 4 MIMO antenna system, respectively. ECCs lower than 0.01 within the desired band are achieved for both the single-handhold and double-handhold scenarios. The efficiencies of ANTs 2 and 4 shown in Fig. 16 decrease to 60% due to the hands effect, but it still can satisfy the antenna requirement from industrial mobile terminal applications.

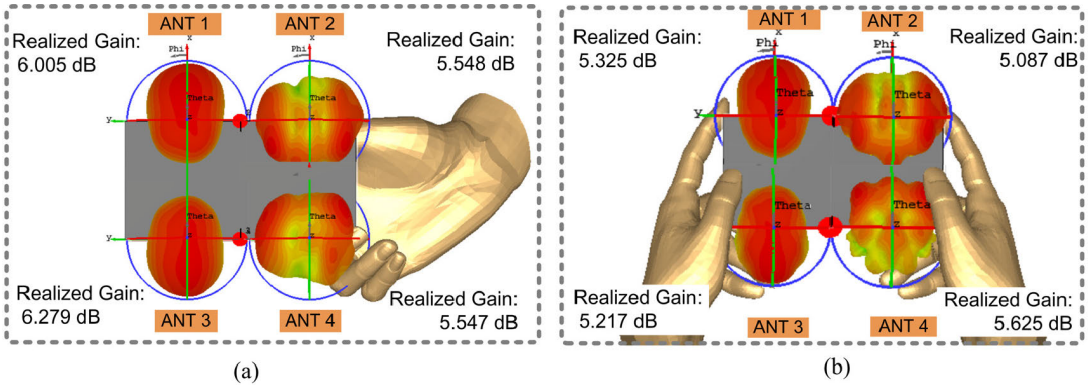

FIGURE 13. Simulated model of handhold scenarios for the proposed 4 × 4 MIMO antenna system: (a) single-handhold; (b) double-handhold.

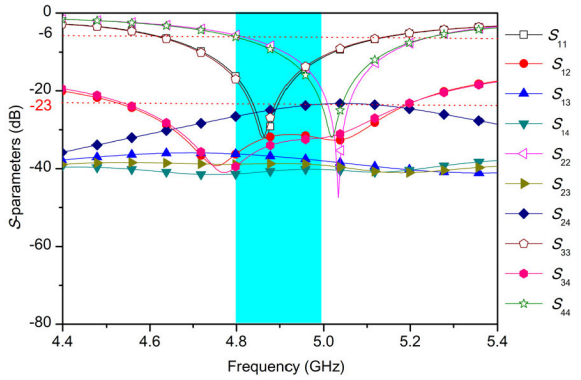

FIGURE 14. Simulated S-parameters of the proposed 4 × 4 MIMO antenna system with single-handhold.

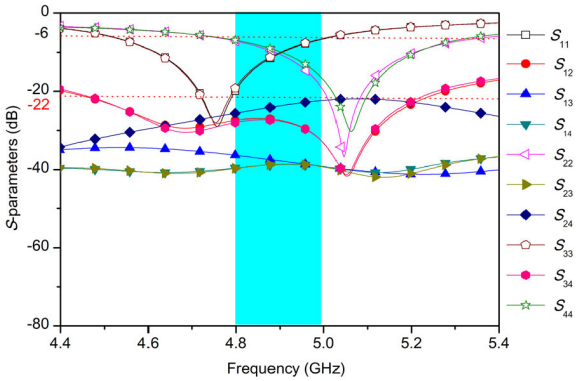

FIGURE 15. Simulated S-parameters of the proposed 4 × 4 MIMO antenna system with double-handhold.

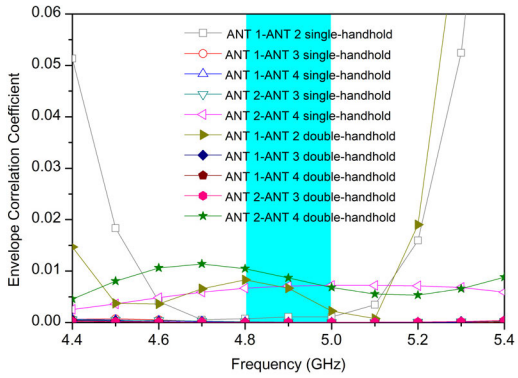

FIGURE 16. Simulated ECCs of the proposed 4 × 4 MIMO antenna system with consideration of user's hand effect.

For the 4 × 4 MIMO antenna system in this work, it is purposely to arrange the proposed antennas away from the user's hands, which makes the antenna performance less sensitive to the hands effect.

III. ANTENNAS ARRANGEMENT DISCUSSION

The proposed 4×4 MIMO antenna system has been evaluated in last section. In the case of antenna arrangement shown in Fig. 1, the MIMO antenna system obtains isolation better

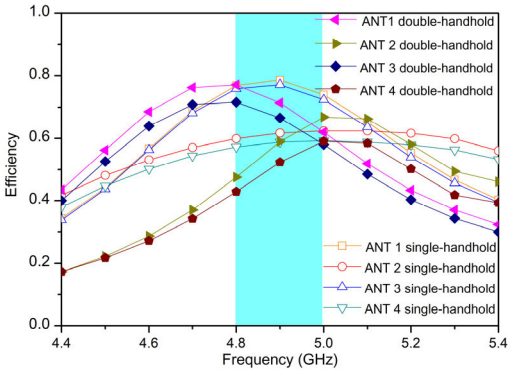

FIGURE 17. Simulated efficiencies of the proposed 4 × 4 MIMO antenna system with consideration of user's hand effect.

than 25 dB, ECC lower than 0.01 and efficiency up to 80%, as well as complementary radiation patterns. User's hands effect on the proposed structure has also been discussed. Here, further discussion on the antenna arrangement for the MIMO antenna system is necessary to study so as to validate the versatility of the proposed co-located antenna pairs and the self-neutralization decoupling method.

For the handset structure proposed in the paper, more antenna pairs can be arranged along the longer walls of the handset frame. Fig. 18 shows another two possible scenarios of 8 × 8 and 10 × 10 MIMO antenna systems. For these arrangements, the distance between the adjacent loop antenna and the antenna pair is 60 mm and the antennas are located symmetrically along the longer walls of the handset.

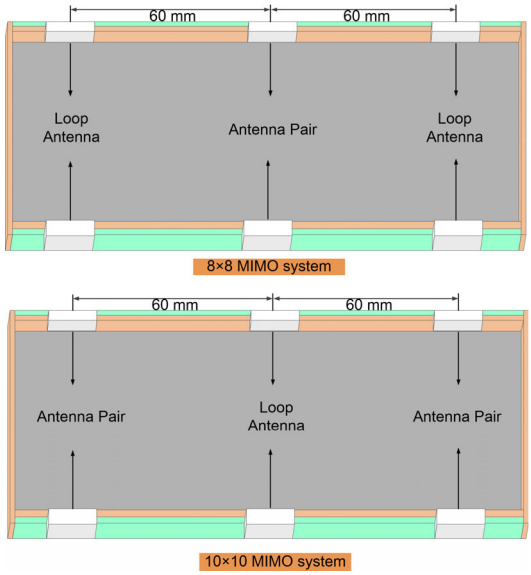

FIGURE 18. The 8 × 8 MIMO (case 1) and 10 × 10 MIMO antenna systems (case 2).

For the 8 × 8 MIMO antenna system, two antenna pairs are placed at the center of the longer walls with other four loop antennas 60 mm away from the antenna pairs. Here, "8" stands for 4 ports from the two antenna pairs with

additional 4 ports from the four loop antennas. While exchanging the locations between the antenna pairs and the loop antennas in the 8 × 8 MIMO antenna system, a 10 × 10 MIMO antenna system can be formed within the same handset size. Evaluation of the 8 × 8 MIMO antenna system (case 1) is carried out firstly to ensure the MIMO performance. Along the longer walls, ANT 1 (loop antenna), ANT 2 (loop antenna), ANT 3 (monopole antenna) and ANT 4 (loop antenna) are located orderly. *S*-parameters and efficiencies of the proposed case 1 are shown in Figs. 19 and 20. Note that only antennas along one of the longer walls have been studied due to the symmetry of the antenna arrangement. The isolation of the 8 × 8 MIMO antenna system is better than 20 dB and the ECCs are lower than 0.01, showing this arrangement is sufficient to achieve good MIMO performance.

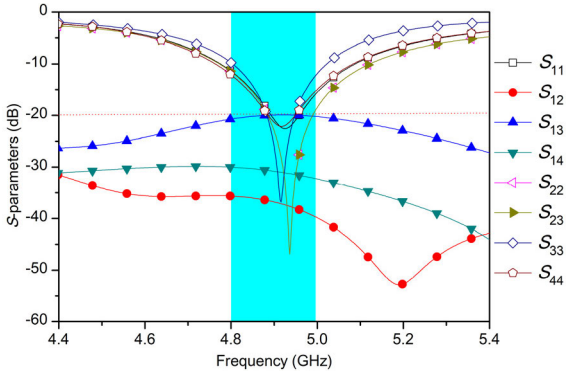

FIGURE 19. Simulated S-parameters of the proposed 8 × 8 MIMO antenna system (case 1).

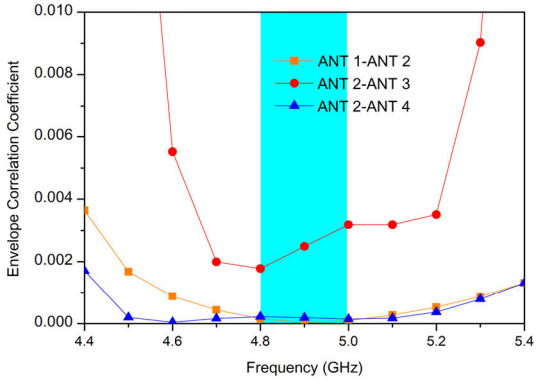

FIGURE 20. Simulated ECCs of the proposed 8 × 8 MIMO antenna system (case 1).

In the case of 10 × 10 MIMO antenna system (case 2), it consists of an antenna pair (ANT 1: loop antenna, ANT 2: monopole antenna), a loop antenna (ANT 3) and another antenna pair (ANT 4: loop antenna, ANT 5: monopole antenna) along one longer wall of the handset frame. The isolations and ECCs are also studied and shown in Figs. 21 and 22. Considering the symmetry of the antennas arrangement, only the ANTs 1-5 are chosen to illustrate the isolation performance of the 10 × 10 MIMO antenna system.

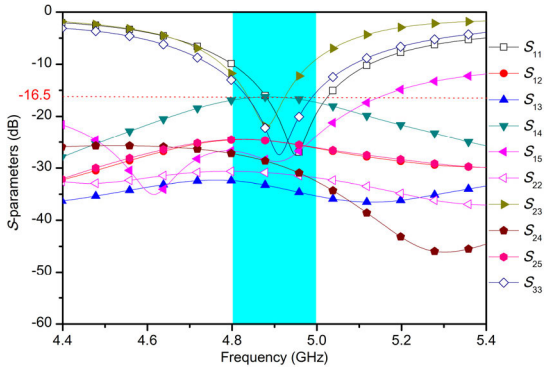

FIGURE 21. Simulated S-parameters of the proposed 10 × 10 MIMO antenna system (case 2).

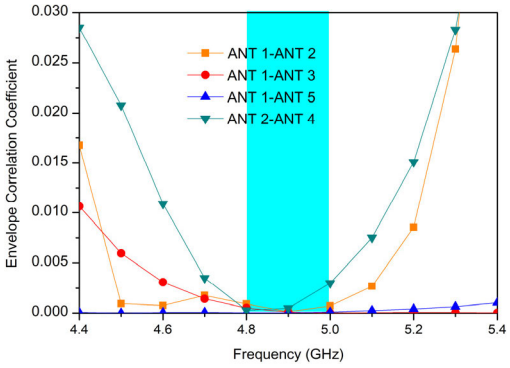

FIGURE 22. Simulated ECCs of the proposed 10 × 10 MIMO antenna system (case 2).

As shown in Fig. 21, except S_{14} is lower than −16.5 dB within the desired band, other transmission coefficients are better than −25 dB. Only ECCs between ANT 1-ANT 2, ANT 1-ANT 3, ANT 1-ANT 5 and ANT 2-ANT 4 are calculated to represent the radiation isolation performance. The ECCs between the antennas of the same pair and the same antenna type are studied because their corresponding results are more likely the highest/worst values among all the ECCs, which are the typically values to represent the performance of the proposed MIMO antenna system. Overall, ECCs lower than 0.03 are obtained within the band of 4.8 GHz-5.0 GHz as shown in Fig. 22.

According to the above discussion about the arrangement of the MIMO antenna system, isolation better than 20 dB/16.5 dB can be obtained for the 8 × 8.10 × 10 MIMO antenna systems respectively. ECCs lower than 0.01/0.03 are also achieved, ensuring the proposed 8 × 8.10 × 10 MIMO antenna systems have promising complementarity in radiation patterns for larger channel capacity.

Finally, the impacts of the LCD module and battery are also discussed by simulation. The simulated *S*-parameters with the above-mentioned components are listed in Figs. 23 (a) and (b). The LCD module is covered on the vertical walls of the handset, which is made of glass (relative permittivity: 7 and loss tangent: 0.02). And the dimension of the battery is 60 × 120 mm^2, as illustrated in Fig. 23.

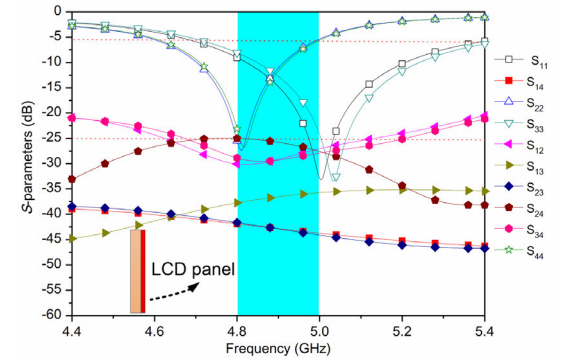

(a) Simulated *S*-parameters of optimized antenna pair with LCD

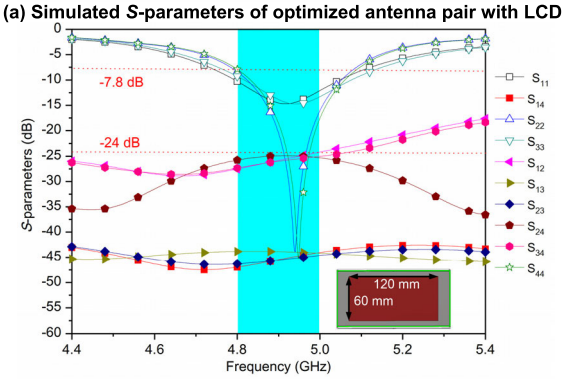

(b) Simulated *S*-parameters of optimized antenna pair with battery

FIGURE 23. Simulated impacts of LCD and battery.

Also, the simulated efficiencies with LCD module and battery are shown in Fig. 24. Although the slight frequency shifts have been observed compared with Fig. 9, they can be tuned during the antenna design process. Also, the components exert negligible impacts on the peak efficiencies, as depicted in Fig. 24. And the total efficiency drops within the operating band are caused by the frequency shifts.

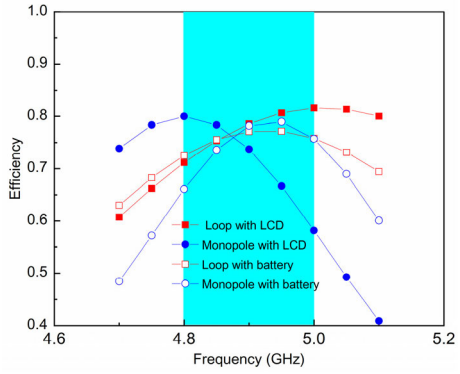

FIGURE 24. Simulated efficiencies with LCD/battery.

IV. EXPERIMENTAL RESULTS

To experimentally verify the performance of the proposed antenna pairs and the corresponding 4 × 4 MIMO antenna system, a prototype was fabricated and measured, as shown in Fig. 25. Four coaxial cables are adopted to feed the antennas and their losses have been taken into consideration

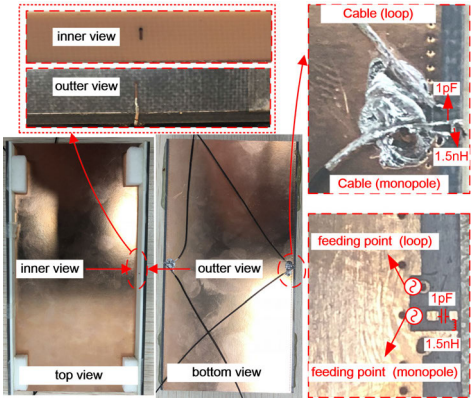

FIGURE 25. Prototype of the proposed 4 × 4 MIMO antenna system.

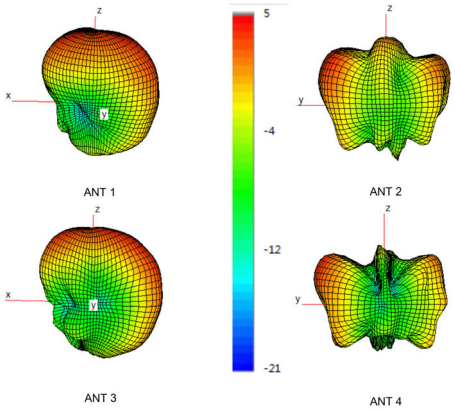

FIGURE 26. Measured radiation patterns at 4.9 GHz.

during the measurement. To show the practical experimentations of the 4 × 4 MIMO antenna system, the *S*-parameters, the radiation efficiencies, the radiation patterns and ECCs are demonstrated below.

The measured radiation patterns at 4.9 GHz for ANTs 1, 2, 3 and 4 are illustrated in Fig. 26, which are in good agreement with the calculated patterns shown in Fig. 10. The simulated and measured *S*-parameters as well as the efficiencies of the proposed prototype are presented in Figs. 27 and 28 respectively, from which one can observe the simulated and

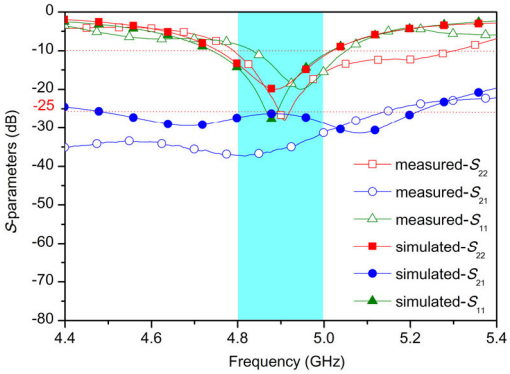

FIGURE 27. Measured and simulated *S*-parameters of the ANTs 1 and 2.

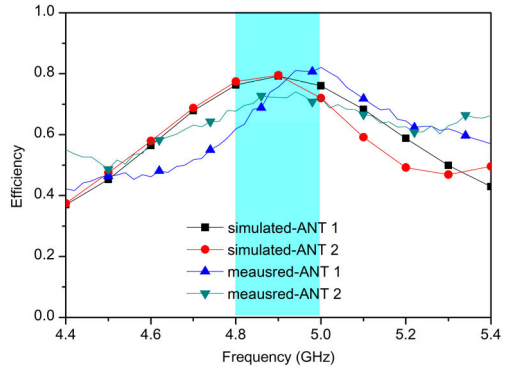

FIGURE 28. Measured and simulated efficiencies of the ANTs 1 and 2.

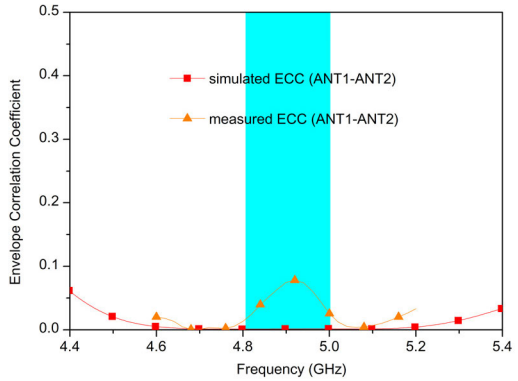

FIGURE 29. Measured and simulated ECCs of the ANTs 1 and 2.

the measured results well coincide with each other. As the aforementioned analysis of the 4 × 4 MIMO antenna system shows that the coupling level between the same antenna pairs can typically represent the isolation performance of the proposed antenna, only S_{11}, S_{21} and S_{22} are tested during the measurement. Results show that better than 25 dB isolation can be obtained within the desired operating band. Also, only efficiencies of the ANT 1 and the ANT 2 are presented to verify the radiation performance of the proposed 4 × 4 MIMO antenna system due to the symmetry of the antenna pairs' arrangement. Fig. 28 shows antenna efficiencies ranging from 60% to 80% have been experimentally achieved. Moreover, the ECC between the ANT 1 and the ANT 2 (the same antenna pair) is post-processed using the measured far-field radiation data following the equations (1) and (2), which is shown in Fig. 29. And the measured ECC lower than 0.1 is achieved within the desired bandwidth.

V. CONCLUSION

Self-neutralization decoupling technique is proposed in the paper to achieve high isolation performance for the co-located antenna pairs. Compact size (50%) and better isolation performance are obtained simultaneously for the antenna pairs without any additional decoupling structure, which is of great significance for the industrial handset antenna applications. Additionally, complementary radiation patterns can be realized by the antenna pairs, which greatly contribute to a lower ECC value and better MIMO performance. Also, little ground clearance is needed at the ground plane of the handset. To completely verify the proposed antenna pairs to be a good candidate for 5G MIMO antenna system, a 4 × 4 MIMO antenna system was studied taking the user's hands effect into account. Moreover, the co-located antenna pairs can be placed at the centers of the longer walls of the handset frame, which is greatly beneficial to reduce both the single-handhold and double-handhold influences on the antenna performance. In the future, the proposed co-located antenna pairs and the 4 MIMO antenna system could be utilized for 5G mobile terminals to achieve decent MIMO performance and better users' experience, considering that part of the N79 band ranging from 4.9 GHz to 5.0 GHz has been assigned to China Mobile Communications for 5G applications by Ministry of Industry and Information Technology of the People's Republic of China.

Furthermore, the 8 × 8 and the 10 × 10 MIMO antenna systems have also been investigated utilizing the proposed antenna pairs. Good isolation performance and satisfactory efficiencies were obtained which could meet industrial requirements for practical applications.

REFERENCES

[1] L. Sun, H. Feng, Y. Li, and Z. Zhang, "Compact 5G MIMO mobile phone antennas with tightly arranged orthogonal-mode pairs," *IEEE Trans. Antennas Propag.*, vol. 66, no. 11, pp. 6364–6369, Nov. 2018.

[2] D. Q. Liu, M. Zhang, H. J. Luo, H. L. Wen, and J. Wang, "Dual-band platform-free PIFA for 5G MIMO application of mobile devices," *IEEE Trans. Antennas Propag.*, vol. 66, no. 11, pp. 6328–6333, Nov. 2018.

[3] J.-J. Liang, J.-S. Hong, J.-B. Zhao, and W. Wu, "Dual-band dual-polarized compact log-periodic dipole array for MIMO WLAN applications," *IEEE Antennas Wireless Propag. Lett.*, vol. 14, pp. 751–754, 2015.

[4] J. Guo, L. Cui, C. Li, and B. Sun, "Side-edge frame printed eight-port dual-band antenna array for 5G smartphone applications," *IEEE Trans. Antennas Propag.*, vol. 66, no. 12, pp. 7412–7417, Dec. 2018.

[5] K.-L. Wong, C.-Y. Tsai, and J.-Y. Lu, "Two asymmetrically mirrored gap-coupled loop antennas as a compact building block for eight-antenna MIMO array in the future smartphone," *IEEE Trans. Antennas Propag.*, vol. 65, no. 4, pp. 1765–1778, Apr. 2017.

[6] M.-Y. Li, Y.-L. Ban, Z.-Q. Xu, G. Wu, C.-Y.-D. Sim, K. Kang, and Z.-F. Yu, "Eight-port orthogonally dual-polarized antenna array for 5G smartphone applications," *IEEE Trans. Antennas Propag.*, vol. 64, no. 9, pp. 3820–3830, Sep. 2016.

[7] Y.-L. Ban, C. Li, C.-Y.-D. Sim, G. Wu, and K.-L. Wong, "4G/5G multiple antennas for future multi-mode smartphone applications," *IEEE Access*, vol. 4, pp. 2981–2988, 2016.

[8] Y. Li, C.-Y.-D. Sim, Y. Luo, and G. Yang, "12-port 5G massive MIMO antenna array in sub-6GHz mobile handset for LTE bands 42/43/46 applications," *IEEE Access*, vol. 6, pp. 344–354, 2018.

[9] S. Zhang, K. Zhao, Z. Ying, and S. He, "Adaptive quad-element multi-wideband antenna array for user-effective LTE MIMO mobile terminals," *IEEE Trans. Antennas Propag.*, vol. 61, no. 8, pp. 4275–4283, Aug. 2013.

[10] A. Diallo, C. Luxey, P. Le Thuc, R. Staraj, and G. Kossiavas, "Study and reduction of the mutual coupling between two mobile phone PIFAs operating in the DCS1800 and UMTS bands," *IEEE Trans. Antennas Propag.*, vol. 54, no. 11, pp. 3063–3074, Nov. 2006.

[11] S.-W. Su, C.-T. Lee, and F.-S. Chang, "Printed MIMO-antenna system using neutralization-line technique for wireless USB-dongle applications," *IEEE Trans. Antennas Propag.*, vol. 60, no. 2, pp. 456–463, Feb. 2012.

[12] A. B. Numan, M. S. Sharawi, A. Steffes, and D. N. Aloi, "A defected ground structure for isolation enhancement in a printed MIMO antenna system," in *Proc. 7th Eur. Conf. Antennas Propag. (EuCAP), Gothenburg*, Apr. 2013, pp. 2123–2126.

[13] C.-Y. Chiu, C.-H. Cheng, R. D. Murch, and C. R. Rowell, "Reduction of mutual coupling between closely-packed antenna elements," *IEEE Trans. Antennas Propag.*, vol. 55, no. 6, pp. 1732–1738, Jun. 2007.
[14] H. Xu, H. Zhou, S. Gao, H. Wang, and Y. Cheng, "Multimode decoupling technique with independent tuning characteristic for mobile terminals," *IEEE Trans. Antennas Propag.*, vol. 65, no. 12, pp. 6739–6751, Dec. 2017.
[15] L. Zhao, L. K. Yeung, and K.-L. Wu, "A coupled resonator decoupling network for two-element compact antenna arrays in mobile terminals," *IEEE Trans. Antennas Propag.*, vol. 62, no. 5, pp. 2767–2776, May 2014.
[16] J. Sui and K.-L. Wu, "Self-curing decoupling technique for two Inverted-F antennas with capacitive loads," *IEEE Trans. Antennas Propag.*, vol. 66, no. 3, pp. 1093–1101, Mar. 2018.
[17] J. Choi, W. Hwang, C. You, B. Jung, and W. Hong, "Four-element reconfigurable coupled loop MIMO antenna featuring LTE full-band operation for metallic-rimmed smartphone," *IEEE Trans. Antennas Propag.*, vol. 67, no. 1, pp. 99–107, Jan. 2019.
[18] V. Plicanic, B. K. Lau, A. Derneryd, and Z. Ying, "Actual diversity performance of a multiband diversity antenna with hand and head effects," *IEEE Trans. Antennas Propag.*, vol. 57, no. 5, pp. 1547–1556, May 2009.
[19] A. A.-H. Azremi, J. Ilvonen, R. Valkonen, J. Holopainen, O. Kivekäs, C. Icheln, and P. Vainikainen, "Coupling element-based dual-antenna structures for mobile terminal with hand effects," *Int. J. Wireless Inf. Netw.*, vol. 18, no. 3, pp. 146–157, Sep. 2011.
[20] J. Ilvonen, O. Kivekas, J. Holopainen, R. Valkonen, K. Rasilainen, and P. Vainikainen, "Mobile terminal antenna performance with the User's hand: Effect of antenna dimensioning and location," *IEEE Antennas Wireless Propag. Lett.*, vol. 10, pp. 772–775, 2011.
[21] A. Zhao and Z. Ren, "Size reduction of self-isolated MIMO antenna system for 5G mobile phone applications," *IEEE Antennas Wireless Propag. Lett.*, vol. 18, no. 1, pp. 152–156, Jan. 2019.
[22] L. Chang, Y. Yu, K. Wei, and H. Wang, "Polarization-orthogonal co-frequency dual antenna pair suitable for 5G MIMO smartphone with metallic bezels," *IEEE Trans. Antennas Propag.*, vol. 67, no. 8, pp. 5212–5220, Aug. 2019.
[23] A. Ren, Y. Liu, and C.-Y.-D. Sim, "A compact building block with two shared-aperture antennas for eight-antenna MIMO array in metal-rimmed smartphone," *IEEE Trans. Antennas Propag.*, vol. 67, no. 10, pp. 6430–6438, Oct. 2019.
[24] L. Chang, Y. Yu, K. Wei, and H. Wang, "Orthogonally-polarized dual antenna pair with high isolation and balanced high performance for 5G MIMO smartphone," *IEEE Trans. Antennas Propag.*, early access, Jan. 9, 2020, doi: 10.1109/TAP.2020.2963918.
[25] Z. Ren, A. Zhao, and S. Wu, "MIMO antenna with compact decoupled antenna pairs for 5G mobile terminals," *IEEE Antennas Wireless Propag. Lett.*, vol. 18, no. 7, pp. 1367–1371, Jul. 2019.
[26] L. Sun, Y. Li, Z. Zhang, and H. Wang, "Self-decoupled MIMO antenna pair with shared radiator for 5G smartphones," *IEEE Trans. Antennas Propag.*, early access, Jan. 20, 2020, doi: 10.1109/TAP.2019.2963664.
[27] L. Sun, Y. Li, Z. Zhang, and Z. Feng, "Wideband 5G MIMO antenna with integrated orthogonal-mode dual-antenna pairs for metal-rimmed smartphones," *IEEE Trans. Antennas Propag.*, vol. 68, no. 4, pp. 2494–2503, Apr. 2020.
[28] M. Zheng, H. Wang, and Y. Hao, "Internal hexa-band folded Monopole/Dipole/Loop antenna with four resonances for mobile device," *IEEE Trans. Antennas Propag.*, vol. 60, no. 6, pp. 2880–2885, Jun. 2012.

CHONG-ZHI HAN received the B.E. and M.E. degrees in electronic information engineering from the Harbin Institute of Technology (HIT), Harbin, China. He is currently pursuing the Ph.D. degree in information and communication engineering with Shenzhen University, Shenzhen, China. His current research interests include the development and application of multiple-input multiple-output antennas and millimetre-wave antenna.

LI XIAO is currently the Dean of the Shenzhen Academy of Information and Communications Technology and the Team Leader of CCSA TC9 WG1 with China Communications Standards Association. His research interests include wireless communication, electromagnetic compatibility, information security, the Internet of Things, and so on. He presided over the formulation of several international standards, more than ten national standards, and more than 30 industry standards.

ZHE CHEN (Member, IEEE) received the B.E. degree in electronic information engineering and the M.E. degree in electronics and telecommunications engineering from Xidian University, Xi'an, Shaanxi, China, in 2012 and 2015, respectively, and the Ph.D. degree in electronic engineering with the City University of Hong Kong, Hong Kong, in 2018. He was a Postdoctoral Follow with the State Key Laboratory of Terahertz and Millimeter Waves, City University of Hong Kong, from 2018 to 2019. He was a Research Assistant with the Information and Communication Technology Center, Shenzhen Research Institute, City University of Hong Kong, Shenzhen, China, in 2015. He is currently an Assistant Professor with the College of Electronics and Information Engineering, Shenzhen University, Shenzhen, Guangdong. His research interests include reconfigurable antennas, dielectric resonator antennas, millimeter-wave antennas, antennas for mobile terminals and 5G applications, and so on. He was a TPC Member of iWEM 2019.

TAO YUAN (Member, IEEE) received the bachelor's and master's degrees from Xidian University, China, and the Ph.D. degree from the National University of Singapore, Singapore. He is currently a Professor with the College of Information Engineering, Shenzhen University, Shenzhen, China. His current research interests include developing novel RF modules and antennas for mobile terminal and 5G applications.